Enzymatically Active Self-Standing Protein-Polymer Surfactant Films Prepared by Hierarchical Self-Assembly

*Kamendra P. Sharma, Andrew M. Collins, Adam W. Perriman, and Stephen Mann**

The design and construction of robust self-supporting protein films with functional properties remains a key challenge in biomaterials research. Protein molecules provide unique structural architectures with desirable materials properties but are highly sensitive to deactivation during film fabrication. These limitations arise predominantly from loss of protein function from surface-induced denaturation, intermolecular aggregation, steric hindrance of active sites, and lack of dynamical freedom imposed by the solid state. As a consequence, conventional protein-based composites and self-supporting films are fabricated primarily for their useful structural and biocompatible properties,[1] and, although biological activity may be retained, it is often different from the native protein. Significantly, a range of fabrication procedures have been employed to increase the mechanical robustness and porosity of protein films. For example, free-standing films of ferritin were prepared by crosslinking with CdSe quantum dots at the oil-water interface,[2] nanoparticles were used in the fabrication of ultrathin nanofiltration membranes of ferritin on metal hydroxide nanostrands,[3,4] and silica nanospheres employed for the preparation of microporous bovine serum albumin membranes,[5] and imprinting of breath figure patterns on silk fibroin films.[6] In addition, highly-extensible elastic films were prepared by isocyanate-crosslinking of artificial extracellular matrix proteins derived from fibronectin and elastin,[7] and robust films consisting of fibrils from amyloidogenic lysozyme and β-lactoglobulin fabricated by self-assembly methods.[8] Given these recent advances in controlling the structure and morphology of cross-linked protein-based films, it should be possible to integrate high levels of native bio-functionality into such materials. In this regard, functional hybrid protein-polymer nanocomposite blended films have been recently produced via co-assembly of diblock copolymers with the fluorescent protein mCherry,[9,10] poly(ethylene glycol) modified heme proteins,[11] or ferritin,[12] indicating that protein structure and function can be retained in the films by hydrophilic interactions at the interface between the diblock copolymer and protein molecules.

Here we report a novel template-free method to prepare robust self-standing protein films based on the hierarchical self-assembly of discrete protein-polymer surfactant conjugates prepared by electrostatically mediated coupling prior to film formation. The molecular constructs are employed as building blocks for the fabrication of an interconnected microstructure of cross-linked hybrid nanoclusters and microparticles. The procedure enables preservation of the near-native protein structure, which gives rise to the retention of optical properties and enzymatic activity in the free-standing, highly hydrophilic films. Specifically, we demonstrate recyclable phosphatase or oxidoreductase behavior and high levels of peroxidase activity.

Self-standing protein-polymer surfactant films consisting of a cross-linked, hierarchical network of interconnecting hybrid nanoclusters were produced via a partial charge-neutralization self-assembly mechanism (**Figure 1**). The nanoscale clusters were prepared by slow addition of the anionic polymer surfactant 4-nonylphenyl-3-sulfopropyl ether ($\mathbf{S_1}$) to an aqueous solution of cationized ferritin (cFn), cationized apoferritin (cApoFn), cationized myoglobin (cMb), cationized alkaline phosphatase (cALP), cationized glucose oxidase (cGO_x) or cationized green fluorescent protein (cGFP) (Experimental and Supporting Information, Figure S1 and Table S1). Dynamic light scattering (DLS) studies of an aqueous dispersion of $\mathbf{S_1}$-cMb gave a mean number average particle hydrodynamic diameter of 126 ± 33 nm (Supporting Information, Figure S2). Similar hydrodynamic diameters were determined for $\mathbf{S_1}$-cALP and $\mathbf{S_1}$-cGFP dispersions (151 ± 19 nm, 134 ± 18 nm respectively), although the hydrodynamic cluster size for $\mathbf{S_1}$-cFn was considerably larger (473 ± 226 nm (Supporting Information, Figure S2).

Self-standing transparent protein-polymer surfactant films ($\mathbf{S_1}$-cMb, $\mathbf{S_1}$-cALP, $\mathbf{S_1}$-cGO_x, $\mathbf{S_1}$-cGFP, $\mathbf{S_1}$-cFn, $\mathbf{S_1}$-cApoFn) were prepared from the nanocluster building blocks by drying the suspensions in a Petri dish placed in a vacuum desiccator in the presence of glutaraldehyde vapour (**Figure 2** and Supporting Information, Figure S3). The films were insoluble in water or aqueous NaCl, as well as organic solvents such as toluene and ethanol. In most cases, the mass fraction of cationized protein in the hybrid films ranged from 35 to 40 wt% (Table S2 in Supporting Information), which equated to an average protein surface charge: polymer surfactant ratio of approximately 2: 1, indicating that half of the potential polymer surfactant binding sites on the surface of the proteins were occupied by $\mathbf{S_1}$ molecules (Supporting Information, Table S1). The mass fraction of protein was higher for the $\mathbf{S_1}$-cALP films (ca. 50 wt%), although the protein surface charge: polymer surfactant ratio remained at ca. 2: 1. In general, the dried protein-polymer surfactant films were glassy and brittle (Figure 2a,c,e,g), but when exposed to water expanded to form flexible transparent materials (Figure 2b,d,f,h, and Supporting Information, Figure S3b,d,e) with a water content of ca. 50–70 wt% (thermogravimetric analysis, Supporting Information, Figure S4; Table S3). These observations were consistent

Dr. K. P. Sharma, Dr. A. M. Collins,
Dr. A. W. Perriman, Prof. S. Mann
Centre for Organized Matter Chemistry
School of Chemistry
University of Bristol
Bristol, BS8 1TS, U.K.
E-mail: s.mann@bristol.ac.uk

DOI: 10.1002/adma.201204161

ADVANCED MATERIALS
www.advmat.de

Materials Views
www.MaterialsViews.com

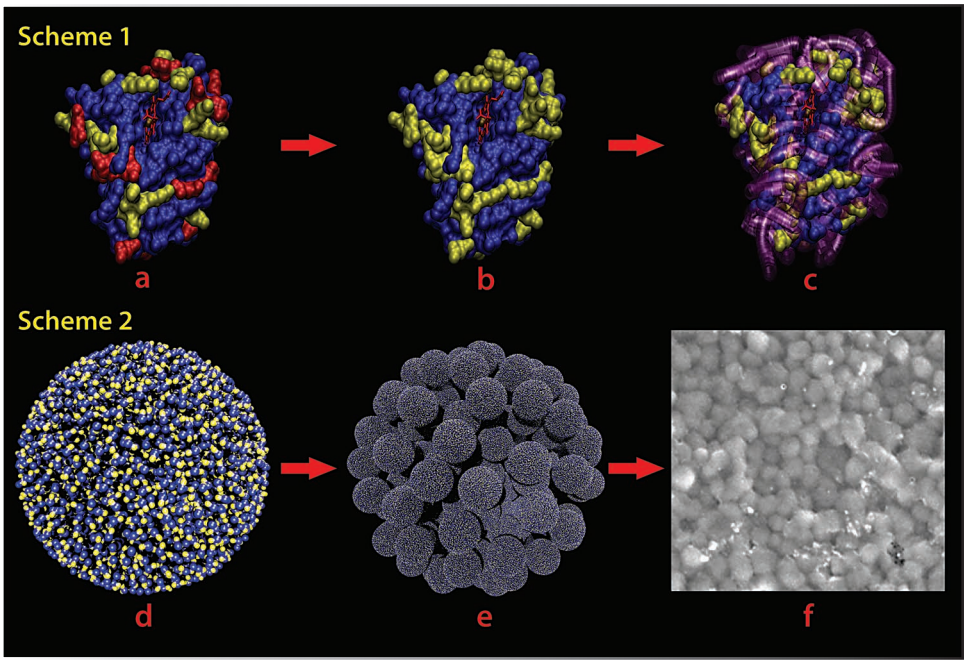

Figure 1. Preparation of protein-polymer surfactant films based on a cross-linked, hierarchical network of interconnecting hybrid nanoclusters. *Scheme 1.* step-wise formation of protein-polymer surfactant molecular building blocks; (a) molecular graphic of myoglobin (Mb) showing solvent-accessible anionic (red) and cationic (yellow) regions on the protein surface, (b) graphic showing cationized myoglobin (cMb) molecule prepared by N-(3-dimethylaminopropyl)-N′-ethylcarbodiimide hydrochloride (EDC) coupling of 3-dimethylaminopropylamine to surface anionic residues of Mb, and (c) graphical representation of a cMb-polymer surfactant conjugate prepared by partial electrostatic neutralization of the surface of cMb with anionic macromolecule $\mathbf{S}_1$. Under the conditions described herein, the conjugates spontaneously aggregate into higher-order structures. *Scheme 2.* Fabrication of protein-polymer surfactant films by hierarchical self-assembly. (d) Graphical representation of a ca. 100 nm-diameter nanocluster comprising closely packed array of self-assembled $\mathbf{S}_1$-cMb molecular conjugates (small yellow and purple dots), (e) higher-order assembly of nanoclusters into ca. 1 μm-sized particles, and (f) SEM image showing porous free-standing, macroscopic protein-polymer surfactant film constructed from interconnected micrometre-sized particles. Formation of (e) and (f) occur by drying the nanoclusters in the presence of glutaraldehyde vapour.

with atomic force microscopy (AFM) nano-indentation experiments, which yielded an average film stiffness of 0.13 ± 0.01 N m^{-1}, much lower than that of a dry film (Supporting Information, Figure S5).

Field emission scanning electron microscope (FEG-SEM) micrographs of the protein-polymer surfactant films showed a cross-linked, hierarchical superstructure comprising an interconnected porous network of 700–900 nm-diameter spheroidal

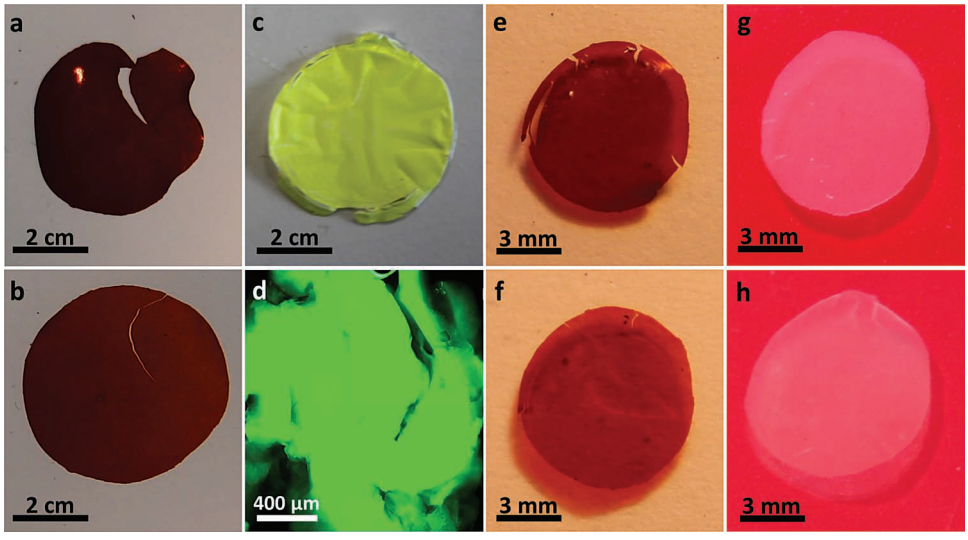

Figure 2. Cross-linked protein-polymer surfactant hybrid films. Optical images of films; (a) dry $\mathbf{S}_1$-cMb, (b) hydrated $\mathbf{S}_1$-cMb, (c) dry $\mathbf{S}_1$-cGFP, (d) fluorescent image of a fragment of a wet $\mathbf{S}_1$-cGFP, (e) dry $\mathbf{S}_1$-cFn, (f) hydrated $\mathbf{S}_1$-cFn, (g) dry $\mathbf{S}_1$-cALP, and (h) hydrated $\mathbf{S}_1$-cALP. Photographs of the $\mathbf{S}_1$-cALP films were taken on a glass slide above red paper to increase the image contrast.

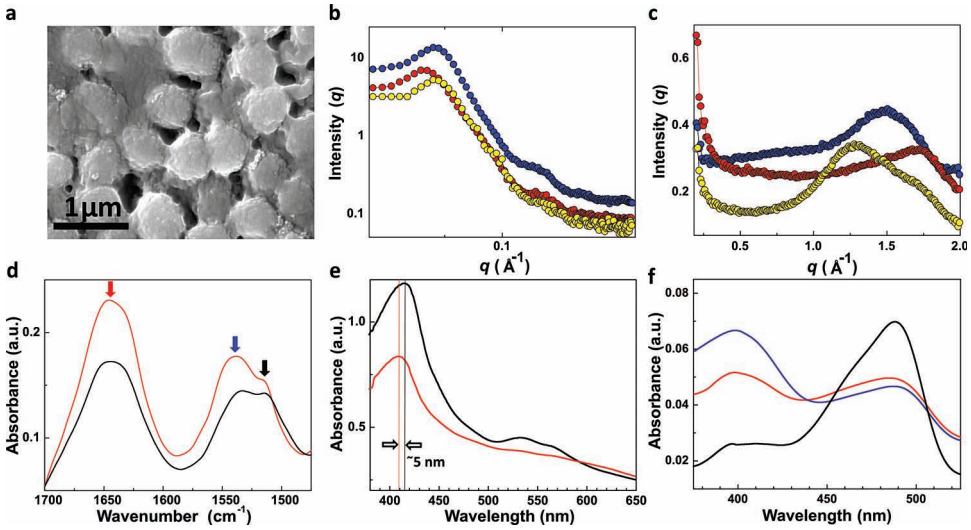

Figure 3. Structure and properties of protein-polymer surfactant nanocluster films. (a) FEG-SEM image from a $\mathbf{S}_1$-cMb hybrid film showing a porous network of interconnected microparticles, with roughened surface texture associated with the self-assembly of a closely packed array of protein-polymer surfactant nanoclusters within each particle. A similar network of cross-linked micron-sized spheroidal particles was observed in $\mathbf{S}_1$-cFn and $\mathbf{S}_1$-cALP films. (b) SAXS or (c) WAXS profiles from dry (blue circles), hydrated (red circles) or toluene-exposed (yellow circles) $\mathbf{S}_1$-cFn hybrid films. (d) ATR-FTIR spectra recorded from a dry $\mathbf{S}_1$-cMb film (black line) and after hydration with H_2O (red line). The red and blue arrows show the positions of the amide I and amide II bands respectively. The surfactant band is shown by black arrow. (e) DR-UV-Vis spectra recorded from a $\mathbf{S}_1$-cMb film showing a 5 nm shift in the Soret band from 414 nm when dry (black line) to 409 nm after hydration (red line). (f) DR-UV-Vis spectra recorded from a $\mathbf{S}_1$-cGFP hybrid film at 25 °C when dry (blue line) or wet (red line) showing change in the ratio of the absorption bands at 395 and 490 nm; corresponding UV-Vis spectrum from a 0.8 mg mL^{-1} aqueous solution of native enhanced GFP in phosphate buffer (pH 7) at 25 °C is also shown (black line).

particles, each of which consisted of a closely packed array of nanoscale clusters ca. 100–200 nm in size (**Figure 3**a). Details of the nanostructure within the particles and clusters were elucidated by using small angle X-ray scattering (SAXS). SAXS profiles for a dry $\mathbf{S}_1$-cFn film showed a feature at $q_d \sim 0.051$ Å^{-1} that corresponded to a protein-protein correlation distance of 12.3 nm (Figure 3b). This distance was only slightly larger than the diameter of equine spleen ferritin (12 nm), which suggested that the ferritin molecules in the nanoclusters were close-packed under anhydrous conditions. Significantly, hydration of the $\mathbf{S}_1$-cFn film resulted in a shift in the position of the peak maximum to $q \sim 0.047$ Å^{-1}, corresponding to an increase in the protein-protein correlation distance to 13.3 nm (Figure 3b). We attributed the film swelling to solvation of the hydrophilic parts of the protein and poly(ethylene glycol) domains of the polymer surfactant, as SAXS experiments performed on the dry $\mathbf{S}_1$-cFn film showed no change in the protein-protein correlation distance after exposure to toluene (Figure 3b). These observations were complemented by wide angle X-ray scattering (WAXS) experiments performed on the $\mathbf{S}_1$-cFn film that showed a decrease in the characteristic alkyl tail-tail intermolecular distances[13] from 4.19 Å (q = 1.50 Å^{-1}) to 3.63 Å (q = 1.73 Å^{-1}) after hydration (Figure 3c), indicative of more effective packing of the hydrophobic surfactant tails as the dielectric constant of the solvent-exposed regions increased. In contrast, analogous WAXS experiments performed on $\mathbf{S}_1$-cFn films exposed to toluene showed an increase in the hydrophobic tail-tail distance to 4.91 Å (q = 1.28 Å^{-1}) (Figure 3c), which confirmed that the hydrophobic tail packing efficiency was highly dependent on solvent polarity. SAXS and WAXS experiments performed on hybrid $\mathbf{S}_1$-cMb and $\mathbf{S}_1$-cALP films showed similar structural responses to hydration (Supporting Information, Figure S6a-c and Table S4). The above results indicated that although the hybrid films were cross-linked via glutaraldehyde-derived bridges,[14] there was sufficient dynamical freedom between the protein molecules to enable considerable displacement of both biomolecular and polymer surfactant components of the interconnected network in response to hydration. The wetting and swelling properties of the films was attributed in part to the use of glutaraldehyde vapour under conditions of slow drying, as films prepared by direct immersion in glutaraldehyde solutions produced materials that showed only minimal solvent-dependent behaviour.

A range of spectroscopy studies were undertaken to ascertain the effects of nanocluster assembly and film formation on the molecular structure of their constituent proteins. ATR-FTIR spectra recorded from dry hybrid protein-polymer surfactant films showed amide I and amide II bands with peak positions that were consistent with the secondary structure distributions of their respective native proteins (Supporting Information, Figure S7 and Table S5). For example, ATR-FTIR spectra of dry $\mathbf{S}_1$-cMb showed well-resolved symmetrical amide I and amide II bands at 1652 cm^{-1} and 1540 cm^{-1}, respectively, which signified that the Mb secondary structure remained predominately α-helical;[15] hydration of the film with H_2O did not have any significant effect on the amide I and II peak positions (Figure 3d). Synchrotron radiation circular dichroism (SRCD) on dry $\mathbf{S}_1$-cALP or dry $\mathbf{S}_1$-cGFP hybrid films showed minima at 212 and 223 nm, or at 218 nm, respectively (Supporting Information, Figure S8), signifying the persistence of the $\alpha\beta$ ALP

secondary structure or near-native GFP β-barrel structure in the protein-polymer surfactant hybrid films. Interestingly, temperature-dependent SRCD spectra of the dry $\mathbf{S_1}$-cALP films showed very little variation from 25 to 125 °C (Supporting information, Figure S9), indicating minimal perturbation of the secondary structure of the protein under these conditions. Diffuse reflectance UV-Vis (DR-UV-Vis) spectroscopy studies on dried $\mathbf{S_1}$-cMb film showed an intense Soret band at 414 nm (low-spin heme metallocentre group of met-Mb),[16] as well as Q_α and Q_β bands at 535 and 570 nm, respectively; hydration of the film at room temperature resulted in a blue shift of the Soret band to 409 nm, corresponding high spin met-Mb under normal aqueous conditions[17] (Figure 3e). These results indicated that solvation of the protein structure in the vicinity of the active site was retained within the $\mathbf{S_1}$-cMb films. Similar DR-UV-Vis spectroscopic studies on dried $\mathbf{S_1}$-cGFP films showed two absorption bands at approximately 395 and 490 nm, with the former showing a ca. 31% reduction in intensity when the films were hydrated (Figure 3f), consistent with a solvent-induced decrease in the degree of protonation of the Tyr 66 residue positioned close to the fluorophorogenic site of the protein.[18]

In light of the persistent levels of protein structure and high hydration capacity of the hybrid materials, enzymatic activities of the $\mathbf{S_1}$-cALP, $\mathbf{S_1}$-cGOx and $\mathbf{S_1}$-cMb hybrid films were assayed at 37 °C (see Supporting Information). In each case, significant levels of enzyme activity were retained in the protein-polymer surfactant hybrid films. For example, the initial rate of peroxidase activity determined for aqueous cMb (0.026 units min^{-1}) was decreased by only 23% for the $\mathbf{S_1}$-cMb films (0.02 units min^{-1}; Supporting Information, Figure S10). The $\mathbf{S_1}$-cALP hybrid film showed effective dephosphorylation of the *p*-nitrophenyl phosphate substrate at an initial rate of 0.08 units min^{-1}, which was 42% of the initial rate of aqueous cALP (0.2 units min^{-1}) (Supporting Information, Figure S11). Similarly, the $\mathbf{S_1}$-cGO_x film also exhibited moderate levels of activity (0.02 units min^{-1}) when coupled with horse radish peroxidase (HRP) in the presence of D-glucose and ABTS [(2,2′-azino-bis(3-ethylbenzothiazoline-6-sulphonic acid)]; this activity was approximately half of the initial rate of oxido-reductase activity determined for aqueous cGO_x (0.05 units min^{-1}) (Supporting Information, Figure S12). Significantly, it was possible to recycle the $\mathbf{S_1}$-cGOx and $\mathbf{S_1}$-cALP hybrid films up to four times with only ~25% and ~31% reductions in the initial rates between the first and fourth cycle, respectively (**Figure 4**a,b). Conversely, the initial rate of peroxidase activity of $\mathbf{S_1}$-cMb films dropped from 77% of the activity determined for aqueous cMb to 6% after only three cycles (Supporting Information, Figure S13), suggesting that the presence of peroxide in the reaction mixture resulted in damage to the enzyme active site, possibly via removal of the heme metallocentre. Thermal inactivation studies performed on the $\mathbf{S_1}$-cALP films showed that the enzyme was thermally stable up to a temperature of 65–75 °C, which was comparable to the inactivation temperature determined for the native enzyme in aqueous solution (Supporting Information, Figure S14).

A systematic evaluation of the effect on enzymatic activity of the chemical modifications employed in nanocluster and film formation was undertaken by performing a steady-state kinetics study on solutions of ALP, cALP, aqueous dispersions of the $\mathbf{S_1}$-cALP nanoclusters, and $\mathbf{S_1}$-cALP films at a range of

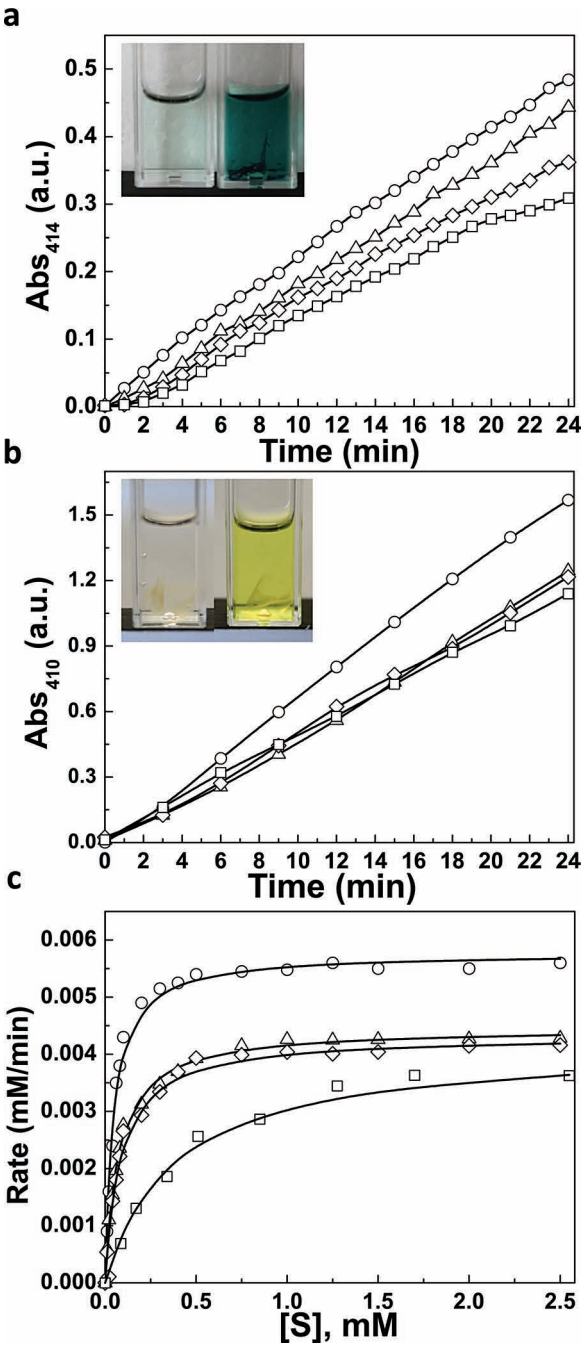

Figure 4. Recyclable enzymatic activity of hybrid protein-polymer surfactant hybrid films. (a) Plot showing initial rates of oxido-reductase activity of a $\mathbf{S_1}$-cGOx film at 25 °C and pH 6.8 over four catalytic cycles (cycle 1: circles; cycle 2: triangles; cycle 3: diamonds; and cycle 4: squares). After each cycle the film was washed and placed in a new D-glucose/ABTS solution and the assay repeated. (b) Comparison of the initial rate of dephosphorylation of *p*-nitrophenyl phosphate due to the presence of $\mathbf{S_1}$-cALP hybrid film at 37 °C and pH 8.8 over four cycles (cycle 1: circles; cycle 2: triangles; cycle 3: diamonds; and cycle 4: squares). The insets in plots (a) and (b) show corresponding changes in colour after formation of the products. (c) Steady-state kinetic assay of the hydrolase activity of a $\mathbf{S_1}$-cALP film (square), aqueous solution of native ALP (circles), aqueous solution of cALP (triangles) and an aqueous dispersion of $\mathbf{S_1}$-cALP hybrid clusters (diamonds) at 37 °C and pH 8.8. Disks of the hybrid $\mathbf{S_1}$-cALP film with masses of 0.06 ± 0.01 mg were used for each substrate concentration.

substrate concentrations (Figure 4c). The initial rates plotted against different substrate concentrations followed Michaelis-Menten kinetics and several parameters, including values for the turnover number (k_{cat}) and Michaelis-Menten constant (K_m) were determined (Table S6 in Supporting Information). The results indicated that covalent coupling of 3-dimethylaminopropylamine to surface anionic residues of ALP resulted in an approximately 23% reduction in k_{cat} for cALP, indicating alterations in the protein structure close to the Ser 102 active site.[19] Indeed, SRCD spectra showed that the α-helical and β-sheet contents increased and decreased from 6 to 8% and 48 to 45%, respectively on cationization (Supporting Information, Figure S8a). In contrast, subsequent conjugation with $\mathbf{S_1}$ to produce dispersed nanoclusters gave only a further 2% reduction in the turnover number. However, higher-order assembly of the nanoclusters into micrometer-sized particles and formation of the self-supporting films via drying in the presence of glutaraldehyde produced a further 28% decrease in turnover number, such that the total reduction in the dephosphorylation turnover rate was ca. 54% when compared with ALP under native conditions. These changes were associated with an approximately fourteen-fold decrease in the magnitude of the specificity constant, k_{cat}/K_m, of the $\mathbf{S_1}$-cALP hybrid films compared to that of native ALP, suggesting that a reduction in the *p*-nitrophenyl phosphate binding affinity occurred possibly via mass transfer resistance.[20] Indeed, we estimate that a substrate molecule would have to diffuse through up to a maximum of 100–200 protein-polymer surfactant layers to reach the active sites of the enzymes located in the centre of the micrometer-sized particles.

Interestingly, decreasing either the concentration or the rate of addition of polymer surfactant, $\mathbf{S_1}$, produced an increase in the nanocluster size (Supporting Information, Figure S15), consistent with a kinetically-driven assembly process in which the termination of nanocluster growth was dependent on steric stabilization and passivation of the aggregate surface by complete polymer surfactant coverage; the latter being more effective at higher $\mathbf{S_1}$: protein molar ratios. Indeed, fast addition at high $\mathbf{S_1}$ concentrations (e.g. addition of 100 mg of pure $\mathbf{S_1}$ to 10 mL of 2 mg mL^{-1} cFn at a rate of >5 mL min^{-1}) produced a high fraction of molecularly dispersed protein-polymer surfactant constructs that could be used to prepare solvent-free liquid proteins.[21–24] Significantly, DLS experiments indicated that the absence of polymer surfactant micelles was a key factor in facilitating nanocluster growth. Whilst no evidence of micelle formation was observed for a 50 mg mL^{-1} solution of $\mathbf{S_1}$ (Supporting Information, Figure S16), micelles were present in a solution of ethylene glycol ethoxylate lauryl ether ($\mathbf{S_2}$) (Supporting Information, Figure S16); the latter failed to produce protein-polymer surfactant nanoclusters when mixed with the cationized proteins. This was not attributed to changing the sulfonate headgroup of $\mathbf{S_1}$ for the carboxylate group of $\mathbf{S_2}$ because nanoclusters and films were produced using glycolic acid ethoxylate 4-nonyl phenyl ether ($\mathbf{S_5}$). Thus, it seems feasible that interactions with the polyanionic $\mathbf{S_2}$ micelles produce a sufficiently high localized surfactant concentration on the surface of the proteins that ensures a higher level of steric stabilization, which as a consequence results in the formation of discrete molecular entities rather than dispersed nanoclusters.

Our results demonstrate that a diverse range of functional biomolecular films can be produced by the hierarchical assembly of ca. 50% charge-neutralized cationized protein-polymer surfactant conjugates. Under these conditions, molecular conjugates can spontaneously self-associate into nanoclusters,[25] which in the studies described above can be self-assembled due to capillary forces when dried in the presence of glutaraldehyde vapour to produce self-supporting films of hierarchically ordered, interconnected micrometer-sized particles. The near-native protein structures and biological activities exhibited by the hybrid films can be reconciled with the soft amphipathic environment created by the polymer surfactant chains electrostatically grafted to the protein surfaces. Indeed, recent studies have shown that poly(ethylene glycol) based anionic surfactant coronas provide an environment that is highly amenable to protein structure, function and dynamics under anhydrous conditions.[21–24] Moreover, the high levels of hydrophilicity (ca. 50–70 wt% H_2O uptake) and the dynamic structural responses of the films upon hydration provide substrate access to the active sites of the nanoclustered enzymes, and a pathway for product release.

Finally, we expect the methodology described herein to contribute significantly to the development of a new class of self-supporting functional hybrid biomaterials, in which the protein molecules serve a dual role in being both an architectural building block as well as a catalyst. Moreover, the high levels of recyclable enzymatic activity exhibited by the wide range of hybrid protein-polymer surfactant films prepared, and the low cost coupled with their ease of fabrication, should have significant implications for the design and construction of new smart biological materials for uses in device fabrication, soft biotechnology and industrially relevant processes of biocatalysis.

Experimental Section

Protein-Polymer Surfactant Hybrid Film Formation: Generally, 1 mL of 50 mg mL^{-1} solutions of $\mathbf{S_1}$ or $\mathbf{S_5}$ at pH 6 were added to magnetically stirred (300 rpm) 10 mL of cationized protein solutions (2 mg mL^{-1}) at a rate of 100 µL min^{-1} using a calibrated syringe pump to yield highly turbid solutions, which were stirred for a further 24 h. Control experiments performed on native proteins showed virtually no turbidity after surfactant addition. The resulting cationized protein-polymer surfactant suspensions were centrifuged at 4200*g*, the supernatant removed, and the resulting precipitate re-suspended in Milli-Q quality water and then centrifuged a second time at 4200*g* to remove any unbound polymer surfactant molecules. The protein-polymer surfactant precipitates were then re-dispersed in 5 mL of Milli-Q quality water and poured into plastic Petri dishes, which were placed in a desiccator (the drying agent used was silica beads along with phosphorus pentoxide; P_2O_5) containing a 5 wt% glutaraldehyde solution. The drying of hybrid clusters was monitored over 36 h and samples were removed once completely dried. The resulting $\mathbf{S_1}$- or $\mathbf{S_5}$-cationized protein hybrid films were removed as self-supporting films from the bottom of the Petri dishes by the addition of small quantities of water, and then placed on thin poly(tetrafluoroethylene) (PTFE) sheets or glass slides.

Supporting Information

Supporting Information is available from the Wiley Online Library or from the author.

Acknowledgements

The authors thank Simon Corcoran for the extensive ray tracing used for model building in Figure 1, Wuge Briscoe for fruitful discussions, Diamond Light Source for access to Beamline B23, Robert Richardson for access to his SAXS and WAXS facility and the EPSRC (Cross-disciplinary interfaces program), Leverhulme Trust and ERC (Advanced Grant) for financial support for A.W.P., K.P.S. and S.M., respectively. The authors also acknowledge support from the Electron Microscopy Unit (EMU) at the School of Chemistry, University of Bristol.

Received: October 4, 2012
Revised: December 6, 2012
Published online: February 5, 2013

[1] C. M. Vaz, M. Fossen, R. F. van Tuil, L. A. de Graaf, R. L. Reis, A. M. Cunha, *J. Biomed. Mater. Res. A* **2003**, *65A*, 60–70.
[2] R. Tangirala, Y. Hu, M. Joralemon, Q. Zhang, J. He, T. P. Russell, T. Emrick, *Soft Matter* **2009**, *5*, 1048–1054.
[3] X. Peng, J. Jin, Y. Nakamura, T. Ohno, I. Ichinose, *Nat. Nanotechnol.* **2009**, *4*, 353–357.
[4] X. Peng, Q. Yu, Z. Ye, I. Ichinose, *J. Mater. Chem.* **2011**, *21*, 4424–4431.
[5] D. Liu, T. Wang, J. L. Keddie, *Langmuir* **2009**, *25*, 4526–4534.
[6] F. Galeotti, A. Andicsova, S. Yunus, C. Botta, *Soft Matter* **2012**, *8*, 4815–4821.
[7] P. J. Nowatzki, D. A. Tirrell, *Biomaterials* **2004**, *25*, 1261–1267.
[8] T. P. J. Knowles, T. W. Oppenheim, A. K. Buell, D. Y. Chirgadze, M. E. Welland, *Nat. Nanotechnol.* **2010**, *5*, 204–207.
[9] B. Kim, C. N. Lam, B. D. Olsen, *Macromolecules* **2012**, *45*, 4572–4580.
[10] C. S. Thomas, M. J. Glassman, B. D. Olsen, *ACS Nano* **2011**, *5*, 5697–5707.
[11] A. D. Presley, J. J. Chang, T. Xu, *Soft Matter* **2011**, *7*, 172–179.
[12] Y. Lin, A. Boker, J. B. He, K. Sill, H. Q. Xiang, C. Abetz, X. F. Li, J. Wang, T. Emrick, S. Long, Q. Wang, A. Balazs, T. P. Russell, *Nature* **2005**, *434*, 55–59.
[13] E. A. Ponomarenko, A. J. Waddon, K. N. Bakeev, D. A. Tirrell, W. J. MacKnight, *Macromolecules* **1996**, *29*, 4340–4345.
[14] I. Migneault, C. Dartiguenave, M. Bertrand, K. Waldron, *BioTechniques* **2004**, *37*, 790.
[15] E. Goormaghtigh, J.-M. Ruysschaert, V. Raussens, *Biophys. J.* **2006**, *90*, 2946–2957.
[16] M. Ikeda-Saito, H. Hori, L. A. Andersson, R. C. Prince, I. J. Pickering, G. N. George, C. R. Sanders, R. S. Lutz, E. J. McKelvey, R. Mattera, *J. Biol. Chem.* **1992**, *267*, 22843–22852.
[17] Q. Li, P. Mabrouk, *J. Biol. Inorg. Chem.* **2003**, *8*, 83–94.
[18] R. Y. Tsien, *Annu. Rev. Biochem.* **1998**, *67*, 509–544.
[19] J. Murphy, B. Stec, L. Ma, E. R. Kantrowitz, *Nat. Struct. Biol.* **1997**, *4*, 618–622.
[20] W. Tischer, F. Wedekind, in *Biocatalysis - From Discovery to Application, Topics in Current Chemistry*, Vol. *200* (Eds: W.-D. Fessner, A. Archelas, D. C. Demirjian, R. Furstoss, H. Griengl, K.-E. Jaeger, E. Morís-Varas, R. Öhrlein, M. T. Reetz, J.-L. Reymond, M. Schmidt, S. Servi, P. C. Shah, W. Tischer, F. Wedekind), Springer, Berlin/Heidelberg, **1999**, pp. 95–126.
[21] A. W. Perriman, H. Cölfen, R. W. Hughes, C. L. Barrie, S. Mann, *Angew. Chem. Int. Ed.* **2009**, *48*, 6242–6246.
[22] A. W. Perriman, A. P. S. Brogan, H. Cölfen, N. Tsoureas, G. R. Owen, S. Mann, *Nat. Chem.* **2010**, *2*, 622–626.
[23] A. P. S. Brogan, G. Siligardi, R. Hussain, A. W. Perriman, S. Mann, *Chem. Sci.* **2012**, *3*, 1839–1846.
[24] F.-X. Gallat, A. P. S. Brogan, Y. Fichou, N. McGrath, M. Moulin, M. Härtlein, J. Combet, J. Wuttke, S. Mann, G. Zaccai, C. J. Jackson, A. W. Perriman, M. Weik, *J. Am. Chem. Soc.* **2012**, *134*, 13168–13171.
[25] E. Dickinson, L. Eriksson, *Adv. Colloid Interface Sci.* **1991**, *34*, 1–29.